CAMBRIDGE
UNIVERSITY PRESS

Article

Wodegongjieite, ideally $KCa_3(Al_7Si_9)O_{32}$, a new sheet silicate isostructural with the feldspar polymorph kokchetavite, $KAlSi_3O_8$

Enrico Mugnaioli[1] (iD), Fahui Xiong[2,3], Xiangzhen Xu[2,3], Mauro Gemmi[4], Richard Wirth[5], Jingsui Yang[6] and Edward S. Grew[7]* (iD)

[1]Department of Earth Sciences, University of Pisa, Via S. Maria 53, 56126 Pisa, Italy; [2]Center for Advanced Research on the Mantle (CARMA), Key Laboratory of Deep-Earth Dynamics of Ministry of Land and Resources, Institute of Geology, Chinese Academy of Geological Sciences, Beijing 100037, China; [3]Southern Marine Science and Engineering Guangdong Laboratory (Guangzhou), 511458, China; [4]Electron Crystallography, Center for Materials Interfaces, Istituto Italiano di Tecnologia (IIT), Viale Rinaldo Piaggio 34, 56025 Pontedera, Italy; [5]Helmholtz Centre Potsdam, GFZ German Research Centre for Geosciences, Section 3.5 Surface Geochemistry, Telegrafenberg, C 120, D-14473 Potsdam, Germany; [6]School of Earth Sciences and Engineering, Nanjing University, Nanjing, 210023, China; and [7]School of Earth and Climate Sciences, University of Maine, Orono, Maine 04469, USA

Abstract

Wodegongjieite occurs in the Cr-11 chromitite orebody of the Luobusa ophiolite in the Kangjinla district, Tibet, China. It is found in two inclusions in corundum: (1) as a partial overgrowth (holotype) up to 1.5 μm thick around a spheroid 20 μm across of wenjiite $(Ti_{10}(Si,P,\square)_7)$, kangjinlaite $(Ti_{11}(Si,P)_{10})$, zhiqinite $(TiSi_2)$ and badengzhuite (TiP), and (2) as pools up to 0.25 μm wide filling interstices between wenjiite, jingsuiite (TiB_2), osbornite–khamrabaevite $(Ti[N,C])$ and corundum. Energy dispersive analyses gave Al_2O_3 34.09, SiO_2 49.11, K_2O 2.56, CaO 11.71, SrO 2.53, total 100.0 wt.%, corresponding to $K_{0.58}Sr_{0.26}Ca_{2.25}Al_{7.20}Si_{8.80}O_{31.20}$, ideally $KCa_3(Al_7Si_9)O_{32}$, for Si + Al = 16 cations.

Single-crystal studies were carried out with three-dimensional electron diffraction providing data for an *ab initio* structure solution in the hexagonal space group *P6/mcc* (#192) with *a* = 10.2(2) Å, *c* = 14.9(3) Å, *V* = 1340(50) Å³ and *Z* = 2. Density (calc.) = 2.694 g·cm⁻³. The refinement, which assumes complete Si–Al disorder, gives average *T*1–O and *T*2–O bond lengths both as 1.65 Å. It was not practical to use unconstrained refinement for the occupancies of the large cation sites 6*f* and 2*a*. The *ab initio* model shows clearly that the two cation sites have different sizes and coordination. Consequently, we imposed the condition (1) that all the K occupies the 2*a* site as the average K–O bond length of 3.07 Å is close to the average K–O bond lengths reported in kokchetavite and (2) that all the Ca occupies the 6*f* site as the average Ca–O bond length of 2.60 Å (2.36 Å and 2.84 Å for Ca–O1 and Ca–O3, respectively) is reasonable for Ca–O. Assuming that all K and all Ca are located at the 2*a* site and 6*f* site, respectively, Sr occupancies of these sites could be refined. Thermal parameters are positive and in a reasonable range. The structure is a sheet silicate isostructural with the K-feldspar polymorph kokchetavite, with two crystallographically distinct sites for K, but not with the topologically identical anorthite polymorph dmisteinbergite $(CaAl_2Si_2O_8)$ with only a single site for Ca. Substitution of K by Ca at the 6*f* site is associated with marked rotation of the Si,Al tetrahedra and a collapse of the structure to accommodate the smaller Ca ion.

The spheroid of intermetallic phases is believed to have formed from the interaction of mantle-derived $CH_4 + H_2$ fluids with basaltic magmas at depths of ∼30–100 km, resulting in precipitation of corundum that entrapped intermetallic melts. Associated immiscible silicate melt of granodioritic composition crystallised metastably to wodegongjieite instead of a mixture of anorthite and K-feldspar.

Introduction

Feldspars are traditionally considered to have the composition MT_4O_8, where M is a large cation such as K, Na or Ca, while T is tetrahedral Al and Si "linked in an infinite three-dimensional

array" (Ribbe, 1983). The feldspar group currently approved by the Commission on New Minerals, Nomenclature and Classification of the International Mineralogical Association (IMA–CNMNC, Back, 2022), constitutes 20 minerals, though three have an overall M:T ratio of 3:8 (for example, banalsite) instead of the more common 1:4, and dmisteinbergite is not included, presumably as it is not a framework silicate (Krivovichev, 2020). In contrast, Krivovichev (2020) proposed that feldspars be considered a family of minerals with the composition $M[T_4O_8]$, thereby following Mills *et al.* (2009, p. 1074),

"mineral families apply to groups and/or supergroups having similar structural and/or chemical features that make them unique." A prime example of a family cited by Mills et al. (2009) is the zeolite family, in which all members are characterised by microporous tetrahedral frameworks with large cavities containing H_2O molecules, although they belong to different groups and supergroups.

Wodegongjieite, ideally $KCa_3(Al_7Si_9)O_{32}$, but with the empirical formula $(K_{0.580}Sr_{0.155}\square_{0.265})(Ca_{0.75}Sr_{0.035}\square_{0.215})_3(Al_{7.2}Si_{8.8})O_{32}$, is, potentially, a new member of the feldspar family as proposed by Krivovichev (2020), being isostructural with kokchetavite ($KAlSi_3O_8$) and topologically identical to dmisteinbergite ($CaAl_2Si_2O_8$), both of which are layered silicates that are polymorphs of sanidine/orthoclase/microcline and anorthite, respectively. Similarly to these two polymorphs, wodegongjieite would be expected to have crystallised metastably in lieu of a feldspar according to Goldsmith's (1953) 'simplexity principle' (e.g. Krivovichev, 2012; 2013; 2020; Zolotarev et al., 2019).

In the present paper, we report a description of wodegongjieite from the type locality and consider how wodegongjieite can be best classified and why wodegongjieite crystallised instead of a mixture of dmisteinbergite and kokchetavite as would be expected from application of Ostwald's step rule together with Goldsmith's (1953) 'simplexity principle'.

The name wodegongjieite is based on the Tibetan name of a famous mountain visible from the area close to the Luobusa chromitite deposit (Fig. 1). This peak is one of the four pre-Buddhist sacred mountains of Tibet and bears the name of the father of all other Tibetan mountain deities. Our choice of spelling is based in part on the pronunciation in Tibetan. Prof. Badengzhu (personal communication) advised us that the Tibetan name of the mountain and the deity associated with the sacred mountain is 'o de gung rgyal: ཝོ་དེ་གུང་རྒྱལ, and that the initial transliterated Tibetan character 'O written in the conventional Tibetan transliteration as the letter O preceded by a right apostrophe, is pronounced 'wo' with the w pronounced as w in 'word', not as v in 'volume'. The Chinese name for the mineral would be 沃德贡杰石, transliterated into English as 'vodegongjieite'. We adopted this pronunciation for the second part of the Chinese name, 贡杰, giving 'wodegongjieite', which is easier to pronounce in English than alternative combinations. Transliteration into Russian is relatively easy: 'водегонгджиеит' as in Russian, as in German, the initial letter would be pronounced 'V' in any case.

Both mineral and name (symbol Wgj) were approved by the IMA–CNMNC (IMA2020-036b, Xiong et al., 2022b). Type material is deposited in the mineralogical collections of the Chinese Geological Museum, Xisiyangrouhutong 15th, Xicheng district, Beijing, China, catalogue number M16104.

Occurrence

Wodegongjieite occurs in the Cr-11 orebody, one of several significant chromitite deposits in the Luobusa ophiolite, Tibet, China (Fig. 2), which is located ∼200 km east-southeast of Lhasa. The Cr-11 orebody (Fig. 3), elevation of 5300 m, is located at 29°11′N, 92°18′E in the Kangjinla district. Wodegongjieite is found in two inclusions (Figs 4–6) of highly reduced compounds enclosed in corundum that was recovered during the processing of 1100 kg of chromitite, described in detail by Xu et al. (2009, 2015). The mineral separation was carried out at the Institute of Multipurpose Utilization of Mineral Resources, Chinese

Fig. 1. (a) 'Vod-de-gung-rgyal' (Wodegongjie) Mountain as seen from the Luobusa ophiolite, Tibet, China. Prof. Jingsui Yang at scientific drilling site LSD-2. (b) Telephoto of 'Vod-de-gung-rgyal' (Wodegongjie) Mountain courtesy of Fahui Xiong. View from south to north.

Academy of Geological Sciences, Zhengzhou. Xu et al. (2009, 2015) reported that before processing, all worksites and equipment were cleaned carefully to avoid contamination. Xiong et al. (2020, 2022a) reviewed the evidence regarding the origin of the corundum and the challenges posed by Litasov et al. (2019a, 2019b) and by Ballhaus et al. (2017, 2018, 2021), and concluded that the majority of data supports a natural and deep-seated origin for the corundum and the minerals included in it.

Wodegongjieite is found in two parageneses. (1) In the holotype sample (foil #5358), it forms a partial overgrowth up to 1.5 μm thick around a spheroid 20 μm across of Ti–Si–P intermetallics (Figs 4 and 5). Associated minerals include zhiqinite, $TiSi_2$ (Xiong et al., 2020), badengzhuite, TiP (Xiong et al., 2020), wenjiite, $Ti_{10}(Si,P,\square)_7$ (Xiong et al., 2022c) and kangjinlaite, $Ti_{11}(Si,P)_{10}$ (Xiong et al., 2022c). Kangjinlaite and wenjiite, constitute about one third of the spheroid (brighter of two phases in the backscattered electron (BSE) image, Fig. 4). Zhiqinite, $TiSi_2$, constitutes much of the remainder of the spheroid (less bright phase in BSE image).

An unidentified phase with the composition SiO_2 53.8, Al_2O_3 16.2, MgO 20.1, CaO 0.3, SrO 2.0, K_2O 7.6, Sum 100 wt.% (uncalibrated energy-dispersive X-ray spectroscopy (EDX) analysis) is also present with wodegongjieite in the overgrowth. The phase could be a milarite (osumilite) group mineral as the a cell parameter 10.1 Å (in hexagonal settings) fits quite well and extinctions appear consistent with $P6/mcc$ symmetry. However, the c
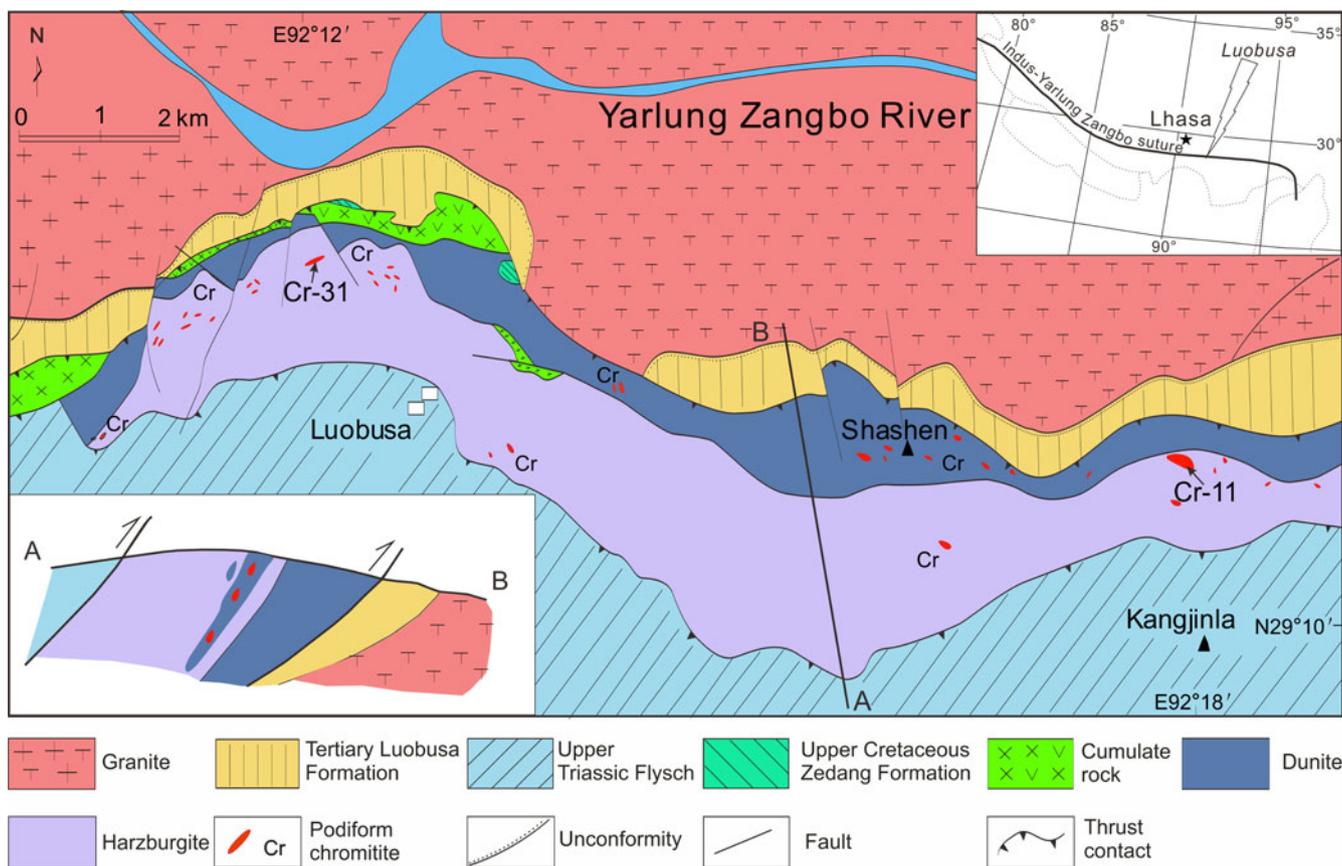
Fig. 2. Map of the Luobusa ophiolite, Tibet, China showing the Cr-31 and Cr-11 chromitite orebodies (stars). Wodegongjieite was recovered from Cr-11. The Zedang Formation is exposed in a small area ~5 km east of the Cr-31 orebody. Map is from Xiong *et al.* (2022a, figure 1). Published with permission from *American Mineralogist*.
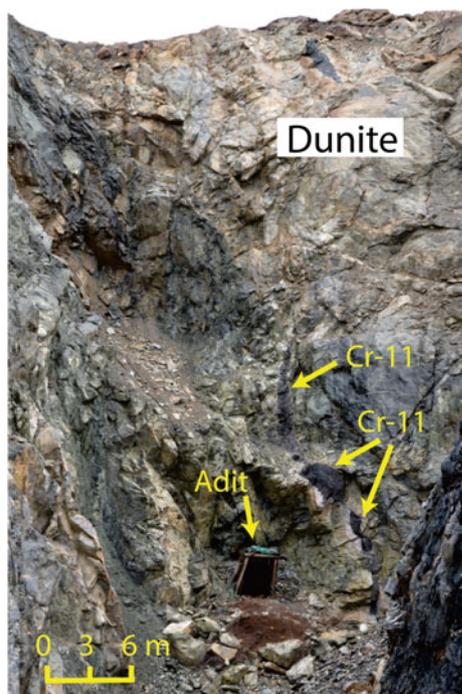

Fig. 3. Exposure showing the Cr-11 chromitite orebody from which wodegongjieite was recovered, Luobusa ophiolite, Tibet, China. The chromitite is enveloped by dunite. From Xiong *et al.* (2020, figure S1(a)).

parameter of 15.6 Å is greater than in most milarite-group minerals (e.g. Armbruster and Oberhänsli, 1988; Gagné and Hawthorne, 2016), even allowing for errors in the measurement. Recalculating the chemical analysis assuming the phase belongs to the milarite group gives $^{A}Mg_2{}^{B}(K_{0.70}Sr_{0.19}Ca_{0.05})_{\Sigma0.94}{}^{C}K$ $^{T(1)}Mg_3{}^{T(2)}(Si_{9.36}Al_{3.31}Mg_{0.23})_{\Sigma12.90}O_{30}$, that is, there is an excess of cations at the *A*, *T*(1) and *T*(2) sites. The unidentified phase and wodegongjieite are close to having parallel orientation, but there is misalignment along *c* of ~10°. Further characterisation of this phase was not possible because the short tilt range and thickness of the sample in this part of the foil preclude obtaining electron diffraction data of sufficient quality.

(2) In foil #6034, wodegongjieite fills interstices up to 0.25 μm wide between wenjiite, jingsuiite, TiB_2 (Xiong *et al.*, 2022a), osbornite–khamrabaevite and corundum (Fig. 6). Identification as wodegongjieite in foil #6034 was confirmed by an EDX spectrum showing the presence of Si, Al, K and Ca, as well as diffraction data indicating that it has the cell of holotype wodegongjieite.

Optical and physical properties

As in the case of the closely related mineral kokchetavite (Hwang *et al.*, 2004), wodegongjieite is too fine-grained for optical and physical properties to be determined. However, it is expected to have some of the properties reported for the next most closely related mineral, dmisteinbergite, from the type locality (Chesnokov *et al.*, 1990; Zolotarev *et al.*, 2019) and from syntheses
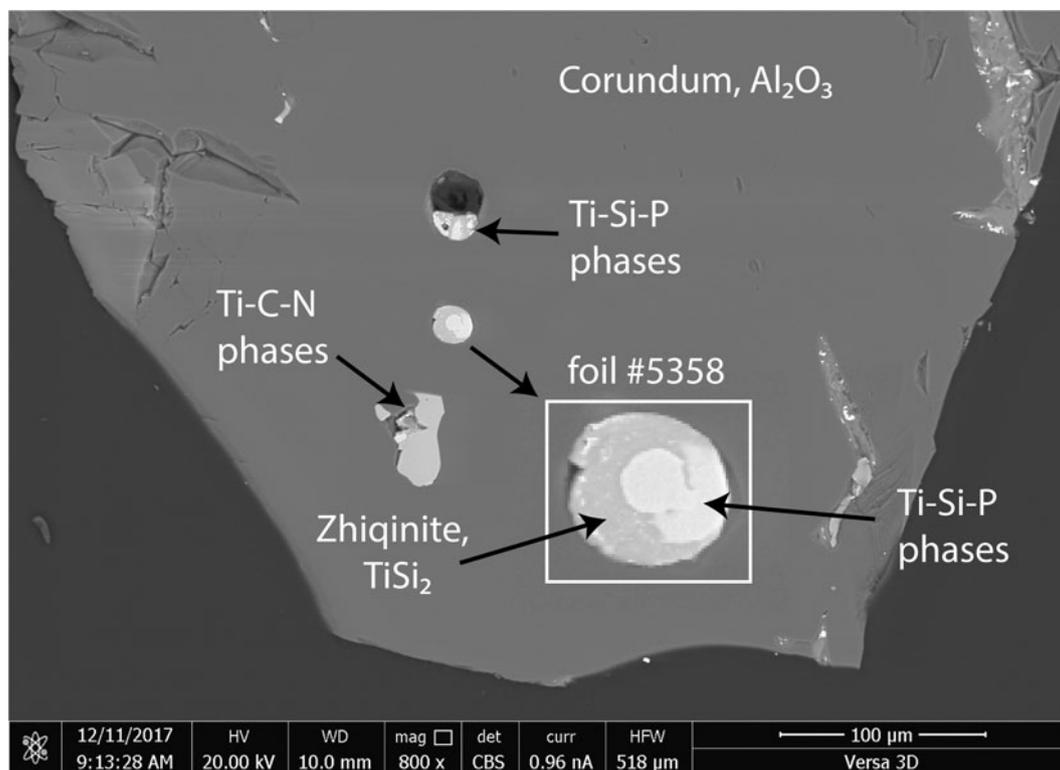
Fig. 4. Back-scattered electron image of the corundum grain showing the source of foil #5358, studied in detail. The inset shows an enlargement of the spheroid composed of $TiSi_2$ (zhiqinite), TiP (badengzhuite), $Ti_{10}(Si,P,\square)_7$ (wenjiite) and $Ti_{11}(Si,P)_{10}$ (kangjinlaite). Images taken at the Center for Advanced Research on the Mantle. From Xiong *et al.* (2020, figure 2).

(Davis and Tuttle 1952), e.g. presumably transparent, uniaxial (+) with birefringence ≈ 0.005 and refractive indices $\approx 1.57–1.59$; colour presumably whitish to colourless; lustre presumably vitreous; Mohs hardness presumably ~6 and tenacity presumably brittle. Density was calculated to be 2.694 g·cm^{-3} from the dynamical structure refinement constrained by the EDX analyses.

Chemical composition

Spectra of wodegongjieite revealed that the major constituents are Al_2O_3, SiO_2, K_2O, CaO and SrO, which were measured with transmission electron microscopy operating at 120 kV and equipped with a Bruker EDX XFlash6T-60 detector. (acceleration voltage = 120 kV). Our EDX uses the thin-specimen approximation by Cliff and Lorimer (1975). Because of the overlap between Si$K\alpha$ and Sr$L\alpha$ lines, the Sr$K\alpha$ lines were used to establish the presence of Sr and to measure its content. Quantification software on an earlier set of four analyses gave a trace of Na in one, but below the 1σ value, and no Na in the other three, and thus the amount of Na was assumed to be below the detection limit. Solution and refinement of the crystal structure did not reveal any evidence for OH, H_2O or CO_2.

Because the EDX analyses were not calibrated with standards, within 9 days of analysing wodegongjieite (Table 1; Supplementary Table S1), we analysed K-feldspar and cowlesite, ideally $KAlSi_3O_8$ and $Ca(Al_2Si_3)O_{10}·5–6H_2O$, respectively, by the same method, that is, also without standards (Supplementary Table S2). No drift is expected to occur over the 9 day interval, as no drift was reported during the 6 months involved in the analysis of wenjiite and kangjinlaite (Xiong *et al.*, 2022c). The standardless EDX analyses gave a good stoichiometry and charge balance for both K-feldspar and cowlesite in terms of the four most abundant constituents, Al, Si, K and Ca if one includes Na in the total for Ca in cowlesite. Although the analyses were not standardised, we are confident that the EDX analyses of wodegongjieite also give a reasonable stoichiometry.

The empirical formula based on the average composition (Table 1) and normalised to Si + Al = 16 cations is $K_{0.58}Sr_{0.26}$ $Ca_{2.25}Al_{7.20}Si_{8.80}O_{31.20}$ (Supplementary Table S1). Although analytical data on the internal standards yielded near ideal charge balance (Supplementary Table S2), the empirical formula shows a deficiency in positive charges: O should be 32. The simplified formula is $(K,\square,Sr)(Ca,\square,Sr)_3(Si,Al)_{16}O_{32}$ and the ideal formula is $KCa_3(Al_7Si_9)O_{32}$, which requires SiO_2 48.59, Al_2O_3 32.06, K_2O 4.23, CaO 15.12, Total 100 wt.%.

Crystallography

Powder X-ray diffraction

It was not possible to obtain a powder X-ray diffraction pattern for this mineral. As this is normally required for new minerals to be approved by the IMA–CNMNC a simulated pattern was obtained (Supplementary Table S3) with GSAS II in Debye Scherrer geometry with a monochromatic Cu$K\alpha$1 radiation (λ = 1.540598 Å) using the software *PowderCell 2.4* (Kraus and Nolze, 1996). The angular limit is 80° (~1.2 Å).

Single-crystal three-dimensional electron diffraction

Method

Three dimensional-electron diffraction (3DED) data (Kolb *et al.*, 2007; Mugnaioli and Gemmi 2018; Gemmi *et al.*, 2019) on wodegongjieite in foil #5358 were collected at the Center for
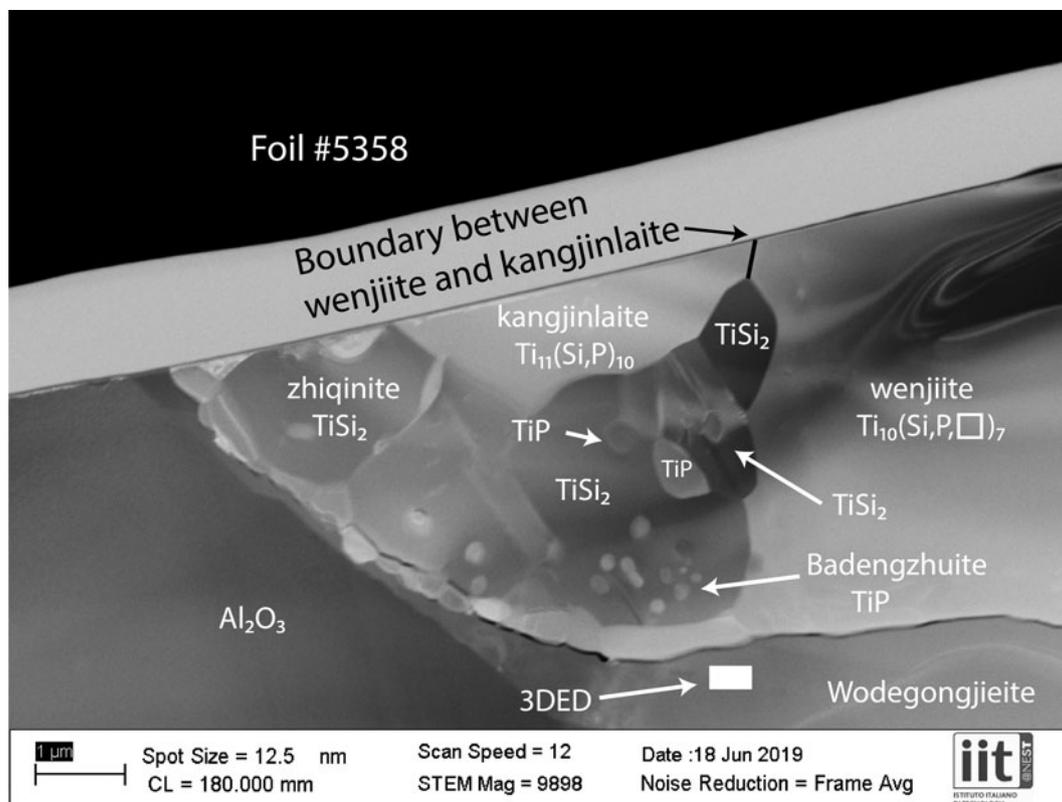
Fig. 5. High-angle annular dark-field scanning-transmission electron microscope (HAADF–STEM) image of foil #5358 showing an aggregate of zhiqinite, $TiSi_2$, several of which have a tabular habit, enclosing globules of badengzhuite, TiP and surrounded by wenjiite ($Ti_{10}(Si,P,\square)_7$) and kangjinlaite $Ti_{11}(Si,P)_{10}$. Al_2O_3 – corundum hosting the Ti silicide inclusion. Seven chemical analyses were obtained within 1 μm of the white rectangle marking the location for collecting the three-dimensional electron diffraction data. The image was obtained at the Istituto Italiano di Tecnologia. Modified from figure 1 of Xiong *et al.* (2022c). Published with permission from *American Mineralogist*.

Nanotechnology Innovation@NEST by a Zeiss Libra TEM operating at 120 kV and equipped with a LaB_6 source and a Bruker EDX detector XFlash6T-60. 3DED acquisitions were performed in STEM mode after defocussing the beam in order to have a pseudo-parallel illumination on the sample. A beam size of ~150 nm in diameter was obtained by inserting a 5 μm C2

Fig. 6. (a) Bright-field and (b) high-angle annular dark-field scanning-transmission electron microscope (HAADF–STEM) images of foil #6034 showing a portion of a lamellar intergrowth of osbornite–khamrabaevite, Ti(C,N), jingsuiite, TiB_2, and wenjiite, $Ti_{10}(Si,P,\square)_7$. Al_2O_3 – corundum hosting the lamellar intergrowth. Wodegongjieite forms pools between corundum and wenjiite, $Ti_{10}(Si,P,\square)_7$. Its identification was confirmed by diffraction data, and the chemical composition is similar to that in foil #5358, but the small size precludes meaningful quantitative analysis. The images were obtained at the GFZ German Research Centre for Geosciences. Modified from figure 7 of Xiong *et al.* (2022a). Published with permission from *American Mineralogist*.

Table 1. Chemical composition (in wt.%) of wodegongjieite in foil #5358.*

Constituent	Mean	Range	S.D.
SiO_2	49.11	47.98–50.93	1.01
Al_2O_3	34.09	33.21–35.20	0.82
K_2O	2.56	2.13–3.04	0.32
CaO	11.71	10.77–12.58	0.58
SrO	2.53	1.88–2.53	0.51
Total	100.00		

*Note: Mean, range and standard deviation (S.D.) of 7 determinations.

condenser aperture. An extremely mild illumination was adopted to avoid any alteration or amorphatisation of the sample.

3DED data were taken in discrete steps of 1° with a precessing beam (Vincent and Midgley, 1994; Mugnaioli *et al.*, 2009) obtained by a Nanomegas Digistar P1000 device. The precession semi-angle was kept at 1°. An in-column Ω-filter was used to filter-out the inelastic scattering contribution. The total tilt range was 90°, slightly limited by the thickness of the FIB lamellae. Camera lengths was 180 mm, with a theoretical resolution limit of 0.75 Å. Electron diffraction data were recorded by an ASI Timepix detector (van Genderen *et al.*, 2016), able to record the arrival of single electrons and deliver a pattern that is virtually background-free. Data were analysed using *ADT3D* (Kolb *et al.*, 2011) for cell and space group determination and for intensity integration. *Ab initio* structure determination and refinement were obtained using direct methods implemented in the software *SIR2014* (Burla *et al.*, 2015). Data were treated with the kinematical approximation (I_{hkl} proportional to F_{hkl}^2).

The structure was refined by taking into account the dynamical effects, as proposed by Palatinus *et al.* (2015a, 2015b, 2017). These authors presented the theory and practice of dynamical refinements of 3DED data, which is now fully implemented in the *PETS2* (Palatinus *et al.*, 2019) and *JANA* software (Petříček *et al.*, 2014). In this procedure, each diffraction pattern is refined separately using Bloch wave formalism. Together with the structure, the sample thickness and the geometrical orientation of each pattern are also refined using a simple platelet model for the sample shape.

Procedure for refining the structure
The 3DED data set collected after energy-filtering the inelastic scattering gave a nice *ab initio* structure solution in the hexagonal space group *P6/mcc* (#192) with $a = 10.2(2)$ Å, $c = 14.9(3)$ Å, $V = 1340(50)$ Å^3 and $Z = 2$ (Fig. 7). The empirical formula was used for modelling except that O was set equal to 32: $K_{0.58}Sr_{0.26}Ca_{2.25}Al_{7.20}Si_{8.80}O_{32}$ instead of 31.20 as calculated from charge balance. The structure was solved *ab initio* by direct methods. The four cation and four oxygen positions were clearly spotted in the first potential map.

The empirical formula was used for the dynamical refinement except that O was set equal to 32: $K_{0.58}Sr_{0.26}Ca_{2.25}Al_{7.20}Si_{8.80}O_{32}$ instead of 31.20 as calculated from charge balance. In an earlier refinement of the structure, we attempted to refine Al and Si occupancy of the tetrahedral sites. An unconstrained refinement gave Si2 to be nearly 100% Si and Si1 to be ~50% Si and 50% Al, whereas the average $T1$–O and $T2$–O bond lengths came out to be 1.66 Å and 1.65 Å, respectively. That is, ordering of Si and Al at the T sites is not evident in the (Si,Al)–O bond lengths.

The current refinement, which assumes complete Si–Al disorder, gives average $T1$–O and $T2$–O bond lengths of 1.65 Å (Table 2, crystallographic information file deposited as Supplementary material),

which are sufficiently close to exclude the possibility of measurable order. These average T–O bond lengths are consistent within the uncertainties of the measurements with a T–O length = 1.673 Å calculated for complete disorder and Si–O = 1.61 Å and Al–O = 1.75 Å for feldspars (Smith and Bailey, 1963). The total charge received by Si1 is somewhat higher than the formal charge, whereas total charge received by Si2 is somewhat lower (Table 3), which could indicate some ordering of Si and Al, but not enough to affect average bond lengths.

In principle, it would be best to refine the occupancies of the large cation sites 6*f* and 2*a* with no assumptions. However, we are dealing with four constituents: Ca, K, Sr and vacancy (□), and such an unconstrained refinement is not practical with electron diffraction data. Nonetheless, the *ab initio* model clearly shows that the 2*a* and 6*f* sites have different sizes and coordination. Consequently, we imposed the condition that all the K occupies the 2*a* site as the average K–O bond length of 3.07 Å is close to the average K–O bond lengths reported in kokchetavite, 3.1453 Å and 3.144 Å for K1–O and K2–O, respectively (Romanenko *et al.*, 2021). We also imposed the condition that all the Ca occupies the 6*f* site as the average Ca–O bond length of 2.60 Å (2.36 Å and 2.84 Å for Ca–O1 and Ca–O3, respectively) is reasonable for Ca–O, e.g. dmisteinbergite has 2.429–2.461 Å (Zolotarev *et al.*, 2019). For the final refinement, Al:Si was fixed to the same ratio for the two tetrahedral sites. K and Ca are fixed to the values from EDX and assigned to the 2*a* and 6*f* sites, respectively. Total Sr was constrained to the EDX value, but free to occupy either the 2*a* site or the 6*f* site or both. We emphasise that K and Ca occupancies were not assumed but determined from the bond lengths. All thermal parameters were refined free of constraints and converge to positive and reasonable values, supporting the correctness of our approach.

Description of the crystal structure.
Wodegongjieite is a sheet silicate (Hawthorne *et al.*, 2019) in which the layers comprise rings of tetrahedra joined alternatively by large cations and apical oxygens (Fig. 8). The structure most closely resembles that of kokchetavite, in which K occupies two sites (Romanenko *at al.*, 2021). One K site is close to perfectly hexagonal (2*a*), whereas the second K site (6*f*) is slightly distorted; six of the distorted rings surround an undistorted ring (Fig. 9). As in kokchetavite, there are two crystallographically distinct sites for the large cations K, Ca and Sr in wodegongjieite. However, substitution of K by Ca at the 6*f* site is associated with marked rotation of the (Si, Al) tetrahedra and a collapse of the structure to accommodate the smaller Ca ion (Fig. 9). Coordination of Ca at 6*f* becomes four short (2.37Å) and four long (2.85Å) Ca–O bonds (Table 3). As viewed down [001], the tetrahedral framework in wodegongjieite resembles a pinwheel consisting of six wings of the tetrahedra coordinated to Ca surrounding a central hexagon around K (Fig. 9).

The collapsed ring around Ca in wodegongjieite differs from the rings surrounding Ca in dmisteinbergite, in which there is only one type of tetrahedral ring and this has a nearly triangular outline (Fig. 9).

Discussion

Distinction of wodegongjieite from closely related minerals and synthetics

The minerals closest to wodegongjieite in terms of crystal structure and composition are dmisteinbergite, $CaAl_2Si_2O_8$, and
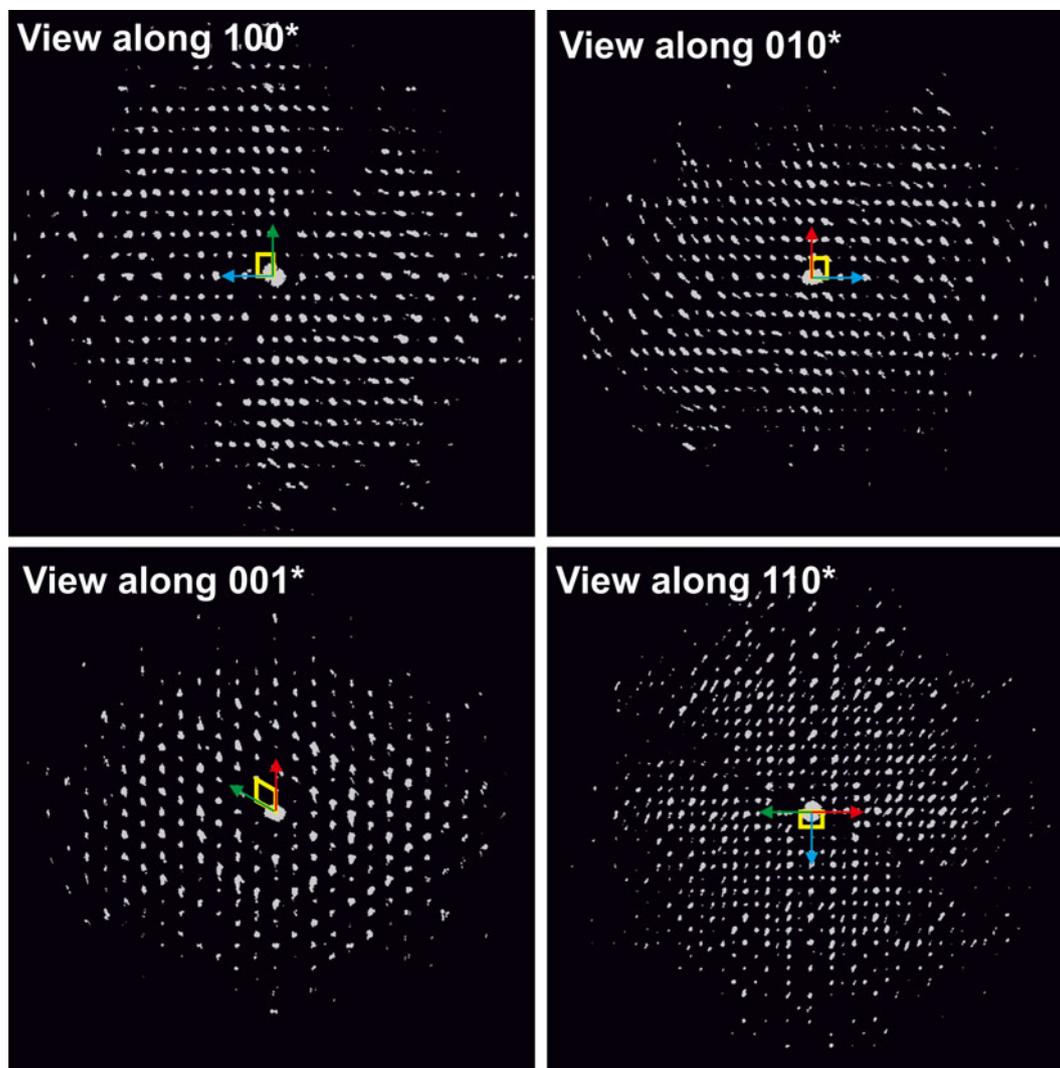
Fig. 7. Three-dimensional reconstruction of electron diffraction data taken from wodegongjieite in foil #5358 (Fig. 4). Cell edges are sketched in yellow. Red arrow indicates $a^\star$ direction, green arrow indicates $b^\star$ direction and blue vector indicates $c^\star$ direction. Note that these panels show projections of a three-dimensional diffraction volume and are not conventional two-dimensional electron diffraction patterns. Each apparent reflection is indeed a column of reflections piled along the viewing direction. Data were obtained at the Istituto Italiano di Tecnologia.

kokchetavite, $KAlSi_3O_8$, both sheet silicates that are polymorphs of feldspar (Hawthorne *et al.*, 2019; Krivovichev, 2020). The recent crystal structure refinement of synthetic kokchetavite (Romanenko *et al.*, 2021) was critical to recognising wodegongjieite as a new mineral distinct from dmisteinbergite and kokchetavite because this refinement enabled comparison of the three minerals with greater clarity as follows:

(1) Wodegongjieite and kokchetavite are isostructural in space group $P6/mcc$ (#192). The two large-cation sites $2a$ and $6f$ are present within each and every layer of both minerals. However, the

Table 2. Coordinates and isotropic displacement parameters (U_{iso}, Å^2) of atoms in wodegongjieite.

Label	x/a	y/b	z/c	U_{iso}	multiplicity	occupancy
K1	0	0	¼	0.0032(19)	2	0.5796
Sr1	0	0	¼	0.0032(19)	2	0.155(8)
Ca2	½	0	¼	0.0020(8)	6	0.75
Sr2	½	0	¼	0.0020(8)	6	0.035(3)
Si1	0.3384(3)	0.1244(2)	−0.10950(15)	0.0025(5)	24	0.55
Al1	0.3384(3)	0.1244(2)	−0.10950(15)	0.0025(5)	24	0.45
O1	0.5131(3)	0.1849(3)	0.1492(2)	0.0039(7)	24	1
O2	0.3342(6)	0.1233(5)	0	0.0096(10)	12	1
Si2	⅔	⅓	0.1094(3)	0.0045(8)	8	0.55
Al2	⅔	⅓	0.1094(3)	0.0045(8)	8	0.45
O3	0.2411(4)	−0.0446(4)	0.1534(2)	0.0135(8)	24	1
O4	⅔	⅓	0	0.016(2)	4	1

Table 3. Polyhedra in wodegongjieite.*

Polyhedron	Composition	Anion	Average bond length	Q	q
Si1	$Si_{0.55}Al_{0.45}$	O1, O2, O3	1.65 Å	4.0	3.6
Si2	$Si_{0.55}Al_{0.45}$	O1, O4	1.65 Å	4.1	3.6
Ca	$Ca_{0.75}Sr_{0.035}\square_{0.215}$	O1	2.36 Å	–	–
Ca	$Ca_{0.75}Sr_{0.035}\square_{0.215}$	O3	2.84 Å	–	–
Ca	$Ca_{0.75}Sr_{0.035}\square_{0.215}$	O1, O3	2.60 Å	1.6	1.6
K	$K_{0.580}Sr_{0.155}\square_{0.265}$	O3	3.07 Å	0.93	0.89

*Note: Q: Total charge received by the ion, q: Formal charge (oxidation number)

two minerals differ in occupancies of the 6*f* site – dominantly Ca in wodegongjieite and entirely K in kokchetavite. Ordering of the layers does not affect this distinction.

(2) Wodegongjieite and dmisteinbergite are not isostructural, although topologically identical. Stacking disorder of the layers in dmisteinbergite can produce two independent Ca sites, but stacked along *c*, whereas the tetrahedral rings around Ca are the same from one layer to the next, albeit rotated relative to one another. Thus, the two sites for large cations in dmisteinbergite are different from the two sites for large cations in kokchetavite and wodegongjieite, which are present in each and every layer.

(3) Converting wodegongjieite to a dmisteinbergite containing 21% $KAlSi_3O_8$ in solid solution with $CaAl_2Si_2O_8$, that is, without changing the bulk K/Ca ratio in wodegongjieite, would require disordering of Ca and K at the 6*f* and 2*a* sites to such an extent that distinction between the two sites would no longer be significant. This requirement seems to be sufficient to distinguish wodegongjieite from a 'potassian dmisteinbergite' containing 21% $KAlSi_3O_8$ in solid solution. Significant $KAlSi_3O_8$ solid solution in dmisteinbergite has not been reported from other localities,

the maximum K_2O reported is 0.12 wt.% (Chesnokov *et al.*, 1990; Simakin *et al.*, 2010; Ma *et al.*, 2013; Fintor *et al.*, 2014, Di Pierro and Gnos, 2016).

(4) Plotting the cell parameters and cell volume versus K/(K+Ca) ratio in dmisteinbergite, wodegongjieite (K/(K+Ca) = 0.21) and kokchetavite yield a nearly perfect linear fit for the *c* parameter (Fig. 10), implying layer thickness is largely influenced by the size of the cations occupying the 6*f* and 2*a* sites. Allowing for the large uncertainties in the cell parameters for wodegongjieite, the plot suggests that the *a* parameter and cell volume for dmisteinbergite plot somewhat above extensions of the lines linking wodegongjieite and kokchetavite, that is, the *P6/mcc* structure with two sites for Ca and K is slightly more compact at a given K/Ca ratio than the *P6₃/mcm* structure with only a single site for Ca and K. In the Ca free-system, the cell volume for kokchetavite is 0.71% smaller than the corresponding cell volume for 'K-cymrite', which like dmisteinbergite, has but a single site for the large cation (Romanenko *et al.*, 2021). However, the small reduction in cell volume on dehydration of 'K-cymrite' to kokchetavite (Fig. 10) differs in that it is achieved through a simultaneous decrease in the *c* cell parameter and increase in the *a* cell parameter.

In summary, the distinction between wodegongjieite and dmisteinbergite is both structural and compositional. Structural because the wodegongjieite has two distinct large-cation sites in each layer, whereas dmisteinbergite has only one such site. Compositional because one of the two sites, namely 2*a*, is occupied dominantly by K in wodegongjieite. That is, wodegongjieite is closer structurally to kokchetavite than to dmisteinbergite despite its being closer to dmisteinbergite in terms of bulk K/(K+Ca) ratio. We have chosen a completely new name 'wodegongjieite' in order to reflect this interpretation of the relationship among the three minerals.
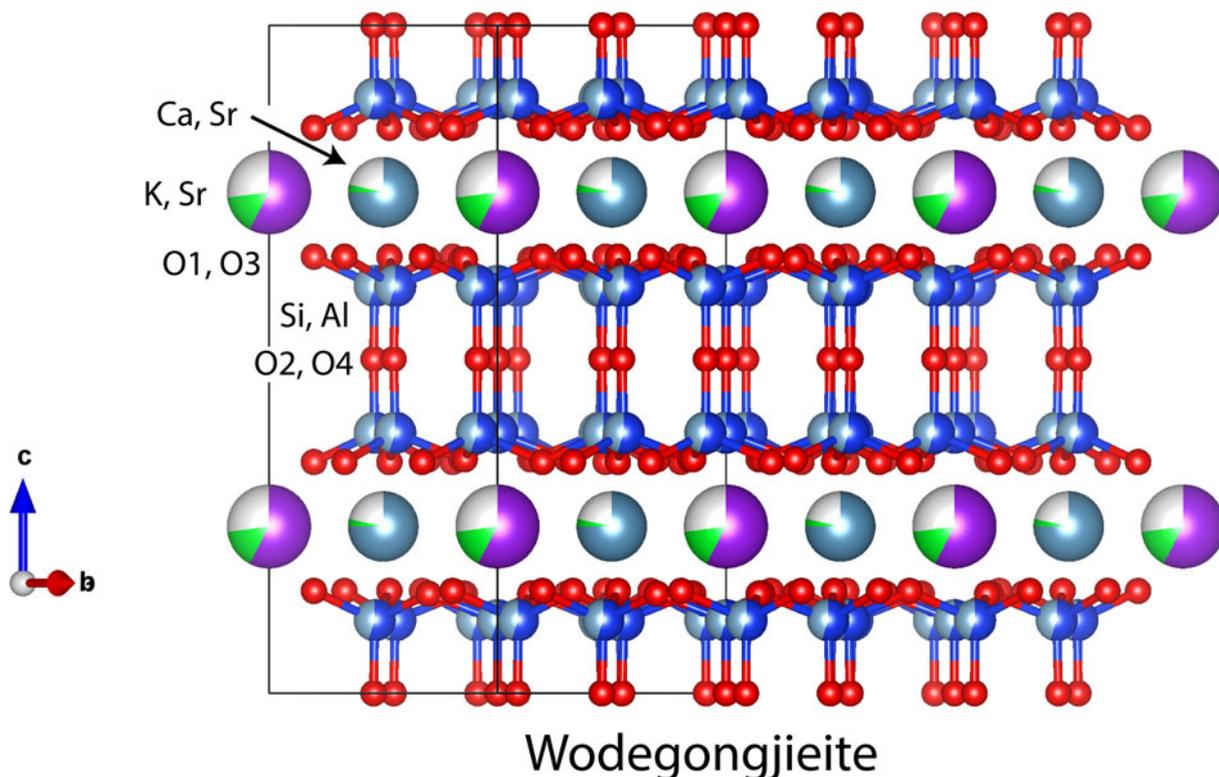

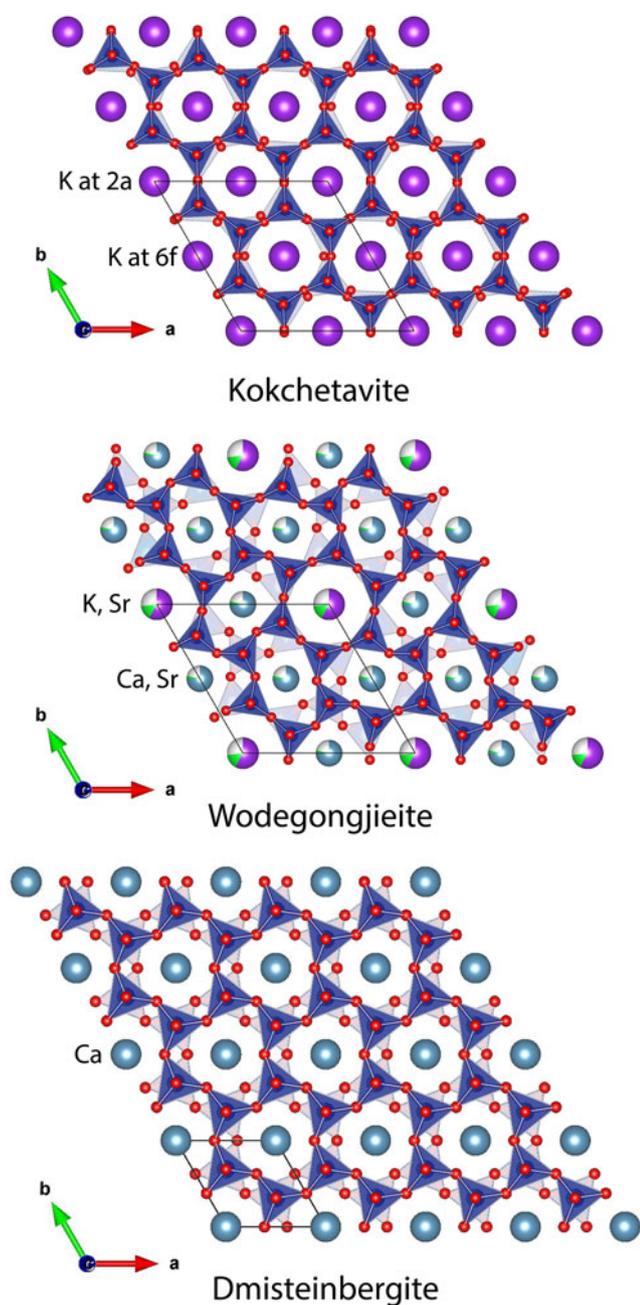**Fig. 8.** View of the wodegongjieite structure along [1$\bar{1}$0]. Drawn using Vesta (Momma and Izumi, 2011).

Fig. 9. Comparison of the wodegongjieite (this study) with kokchetavite (Romanenko et al., 2021) and dmisteinbergite (Dimitrijević et al., 1996) viewed along [001]. The layers for wodegongjieite and kokchetavite were cut for z/c ranging from 0 to 1, whereas that for dmisteinbergite was cut for z/c ranging from 0.25 to 1.25. Drawn using Momma and Izumi (2011).

Wodegongjieite has not yet been synthesised. As far we are aware, kokchetavite has only been synthesised by dehydrating the K-analogue of cymrite, $KAlSi_3O_8 \cdot H_2O$ (Thompson et al., 1998; Kanzaki et al., 2012; Romanenko et al., 2021); no direct synthesis from the oxides or from a melt has been reported.

Conditions of crystallisation of wodegongjieite

Our current scenario for the formation of the six new minerals occurring in and around the spheroid of intermetallic phases in foil #5358 is based on the model developed by Griffin et al.

(2018, 2022) and Xiong et al. (2017) for similar intermetallic phases at Mount Carmel, Israel. Mantle-derived $CH_4 + H_2$ fluids are believed to have interacted with basaltic magmas in the shallow lithosphere (depths of ~30–100 km), which resulted in precipitation of corundum that entrapped intermetallic melts derived from the desilication of a parental magma, presumably basaltic. These intermetallic melts crystallised to Ti–P–Si phases such as the spheroid in foil #5358 (Xiong et al., 2020, 2022) and the aggregate in foil #6034. It is likely that the ternary Ti–Si–P phases in foil #5358 would have crystallised at temperatures below the 1330–1600°C indicated for $TiSi_2$ and TiP, respectively, in the Ti–Si and Ti–P binaries (Xiong et al., 2020, 2022c). Traces of immiscible silicate melt of granodioritic composition (Xiong et al., 2020, 2022c) that is associated with the intermetallic phases crystallised to wodegongjieite, either externally to aggregates of the intermetallic phases in association with an osumilite-like K–Mg–Al–Si–O phase (e.g. the spheroid in foil #5358) or in the interstices between larger crystals of the intermetallic phases (e.g. the aggregate in foil #6034). Potassium, an essential constituent in wodegongjieite, most probably originated in the parental melt and was concentrated in a residual silicate melt after separation of immiscible intermetallic melts.

Classification of wodegongjieite as a feldspar family mineral

Feldspars traditionally are considered to have the composition $M[T_4O_8]$ where M is a large cation such as K, Na or Ca, while T is tetrahedral Al and Si. The feldspar group approved by the IMA–CNMNC (Back, 2022) has just one hierarchical level and comprises 20 minerals, including 11 minerals in the quaternary system relevant for wodegongjieite, $NaAlSi_3O_8$–$CaAl_2Si_2O_8$–$KAlSi_3O_8$–$SrAl_2Si_2O_8$ (Ab–An–Or–Sws), but leaves out one polymorph of anorthite, dmisteinbergite.

Krivovichev (2020) proposed that feldspars are better considered a family that comprises mineral species with the general formula $M^{n+}[T_4^{k+}O_8]$, where n is the average charge of the M^{n+} cation ($n = 1–2$) and k is the average charge of the T^{k+} cation ($k = 4 - n/4$). Banalsite, lisetite and stronalsite would not be included in the feldspar family as M:T = 3:8, not 1:4 (Krivovichev, 2020). Members of the proposed feldspar family would have a crystal structure based upon a d-dimensional network of (TO_m) coordination polyhedra sharing O atoms. For the mineral species known so far, $d = 2$ or 3 (layers or frameworks), and $m = 4$ or 6, i.e. either tetrahedral or octahedral. The feldspar family proposed by Krivovichev (2020) is far better suited for classifying wodegongjieite than is the existing feldspar group approved by the IMA–CNMNC.

Krivovichev's (2020) feldspar family comprises several supergroups based on composition. Minerals in the quaternary system Ab–An–Or–Sws, all belong in the aluminosilicate supergroup, which comprises five groups based on four basic tetrahedral structure topologies and an octahedral topology related to the hollandite structure. Three quaternary feldspar family minerals belong to the last type, while the remaining 10 minerals belong to one of the four groups (Table 4): (1) feldspar topology in the five familiar tectosilicate Ab–An–Or feldspars anorthite, albite, microcline, orthoclase and sanidine (strictly speaking, the last three are not distinct species, but one species with different degrees of Al–Si ordering) (**fsp**); (2) paracelsian topology in the tectosilicate slawsonite (**pcl**); (3) svyatoslavite topology in the tectosilicate svyatoslavite (Krivovichev et al., 2012) and kumdykolite (**bct**); and (4) the dmisteinbergite topology in the sheet silicates dmisteinbergite
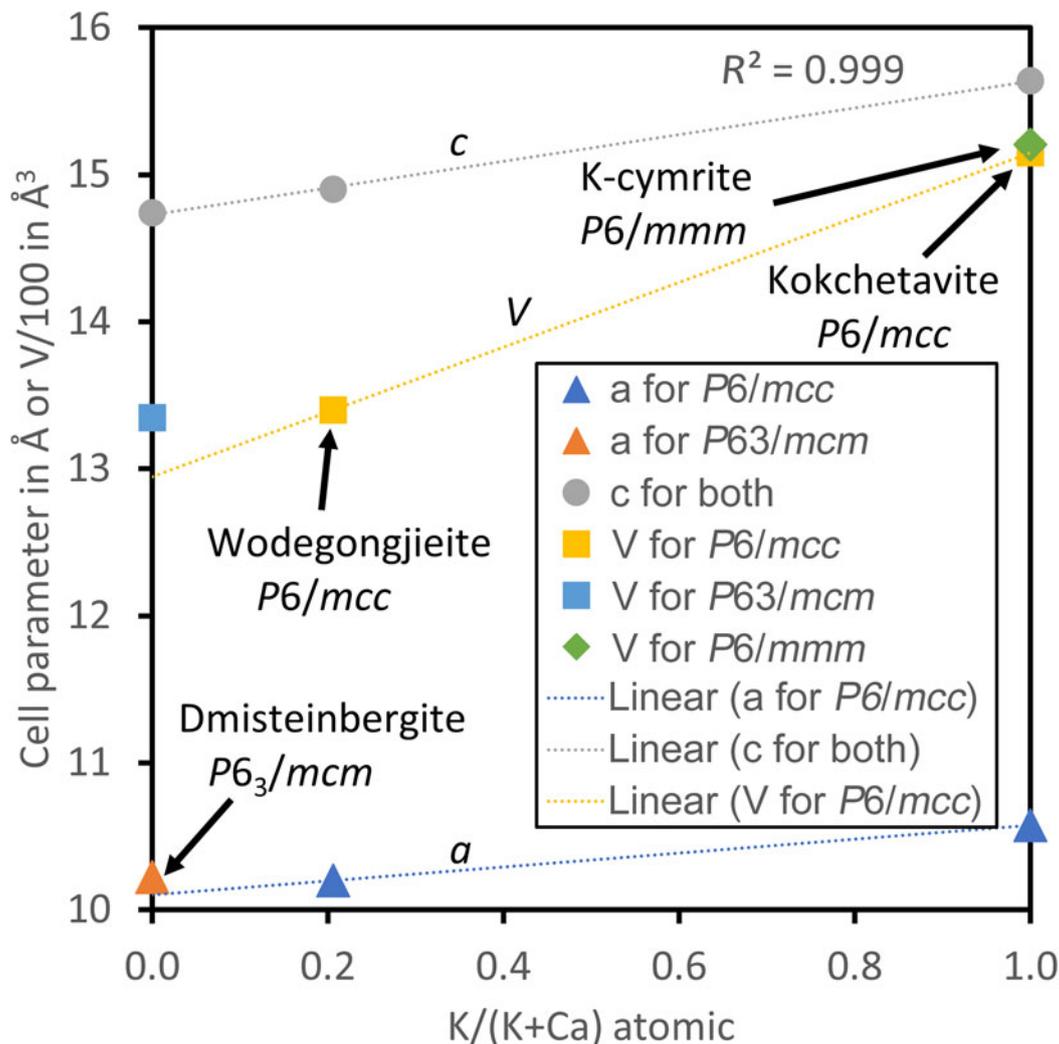
Fig. 10. Plot of cell parameters and volumes of kokchetavite, wodegongjieite, dmisteinbergite and K-cymrite as a function of the K/(K+Ca) ratio. The *a* cell parameter has been doubled and the cell volume quadrupled in dmisteinbergite so as to be directly comparable with the corresponding parameters in wodegongjieite and kokchetavite; those of 'K-cymrite' multiplied 8-fold. The linear fit (R^2 = 0.999) to the *c* parameter applies to kokchetavite, wodegongjieite and dmisteinbergite, whereas the linear fits to the *a* parameter and cell volume apply only to the *P6/mcc* structure. Sources of data are Zolotarev *et al.* (2019), Romanenko *et al.* (2021) and this study for: dmisteinbergite; kokchetavite and K-cymrite; and wodegongjieite, respectively. The parameters reported by Dimitrijevic *et al.* (1996) for synthetic dmisteinbergite (not shown) are close to the plotted values.

and kokchetavite (**dms**). Because wodegongjieite is isostructural with kokchetavite and topologically identical to dmisteinbergite, it can be included in the sheet-silicate group (**dms**).

However, in contrast to these 12 minerals and slawsonite ($SrAl_2Si_2O_8$), the end-member composition for wodegongjieite is intermediate between other feldspar end-members, i.e. 56.2%

Table 4. Shannon information (in bits) in feldspar-family minerals related to wodogongjieite.*

Mineral (space group)	Structural topology	Total mineral		Total framework		Topological framework	
		atom	cell	atom	cell	atom	cell
Anorthite (P1̄)	**fsp**	5.700	592.846	5.585	536.156	2.752	66.039
Sanidine (C2/m)	**fsp**	2.931	76.211	2.752	66.039	2.752	66.039
Microcline (C1̄)	**fsp**	3.700	96.211	3.585	86.039	2.752	66.039
Svyatoslavite (P2₁)	**bct**	3.700	96.211	3.585	86.039	1.545	19.020
Slawsonite (P2₁/c)	**pcl**	3.700	192.423	3.585	172.08	2.252	54.039
Dmisteinbergite (P312)	**dms**	3.046	79.192	2.792	67.020	1.459	17.510
Kokchetavite (P6/mcc)	**dms**	2.637	274.199	2.365	227.020	1.459	17.510
Wodegongjieite (P6/mcc)	**dms**	2.637	274.199	2.365	227.020	1.459	17.510

*Notes: Based on the Shannon information concept (e.g. Krivovichev, 2012, 2013). Structural topologies: **fsp** = feldspar; **bct** = BCT type of zeolite; **pcl** = paracelsian), **dms** = dmisteinbergite (Krivovichev, 2020). Sources of data: slawsonite, svyatoslavite, dmisteinbergite and anorthite (Krivovichev, 2020), kokchetavite calculated from Romanenko *et al.* (2021), wodegongjieite (this study).

$CaAl_2Si_2O_8$, 14.6%, $KAlSi_3O_8$, 6.6% $SrAl_2Si_2O_8$, and 22.6% $\square Si_4O_8$, Moreover, wodegongjieite would be unique among these minerals in showing ordering of two M cations, namely, K and Ca, at two distinct M sites. Other feldspar-family minerals, e.g. kokchetavite, have more than one M site, but only one M cation at these sites.

Metastable crystallisation of wodegongjieite

It is doubtful that equilibrium was attained during crystallisation of wodegongjieite. The equilibrium assemblage expected under the conditions estimated for the spheroid (<1300°C) would comprise K-feldspar and anorthite. Instead, we have a mineral structurally much more closely related to polymorphs of feldspar that are generally considered to have crystallised under non-equilibrium conditions in accord with Ostwald's step rule and Goldsmith's (1953) 'simplexity principle', whereby the least complex polymorphs of a given composition tend to crystallise first, albeit metastably. Complexity is best expressed in terms of the Shannon information concept (e.g. Krivovichev, 2012, 2013, 2020; Krivovichev *et al.*, 2022; Zolotarev *et al.*, 2019). Shannon information in bits reflects diversity of structural sites (information per atom) and both diversity of sites and the number of atoms in the unit cell (information per cell).

Wodegongjieite is structurally simpler than anorthite, but more complex (in terms of total information) than the structurally related dmisteinbergite (Table 4), not surprising given the greater chemical complexity of wodegongjieite compared to dmisteinbergite. The topological complexity of the aluminosilicate layer in wodegongjieite and dmisteinbergite is significantly less than that of the aluminosilicate framework in anorthite and other feldspars. Thus, a theoretical Ostwald sequence for crystallisation of a $CaO–K_2O$-bearing (granodioritic) melt, is predicted to be dmisteinbergite → svyatoslavite → dmisteinbergite + kokchetavite → wodegongjieite → anorthite + sanidine. Note that two minerals, either two feldspars or two feldspar polymorphs, are needed to fully accommodate the major constituents of a granodioritic melt. As far as we are aware, the svyatoslavite stage has not been reported except at the type locality in the Urals. However, the dmisteinbergite + kokchetavite stage has been reported in inclusions of silicate melt (Wannhoff *et al.*, 2022), and the predicted sequence can then be simplified to dmisteinbergite → dmisteinbergite + kokchetavite → wodegongjieite → anorthite + sanidine.

However, the appearance of wodegongjieite without either dmisteinbergite or kokchetavite violates this sequence. A possible explanation is that the tolerance of the wodegongjieite structure for vacancies at the K and Ca sites (the refinement gave 21.5–26.5% vacancy) and the presence of Sr at these sites might have tipped the balance so that wodegongjieite crystallised first despite its greater complexity. Another consideration is that wodegongjieite could have a further advantage in that a single feldspar-family mineral accommodates the granodiorite composition, whereas two feldspar family members with end-member compositions would be needed to accommodate it, that is, one nucleation versus two. The number of phases to be nucleated may only come into play in a very rapid quench, more rapid than the quench of included silicate melt that resulted in the crystallisation of the dmisteinbergite + kokchetavite assemblage reported by Wannhoff *et al.* (2022).

References

Armbruster T. and Oberhänsli R. (1988) Crystal chemistry of double-ring silicates: structural, chemical, and optical variation in osumilites. *American Mineralogist*, **3**, 585–594.

Back M.E. (2022) *Fleischer's Glossary of Mineral Species 2022*. Education Publication Volume 1. Mineralogical Association of Canada, Quebec, Canada.

Ballhaus C., Wirth R., Fonseca R.O.C., Blanchard H., Pröll W., Bragagni A., Nagel T., Schreiber A., Dittrich S., Thome V., Hezel D.C., Below R. and Cieszynski H. (2017) Ultra-high pressure and ultra-reduced minerals in ophiolites may form by lightning strikes. *Geochemical Perspectives Letters*, **5**, 42–46.

Ballhaus C., Fonseca R.O.C. and Bragagni, A. (2018) Reply to Comment on "Ultrahigh pressure and ultra-reduced minerals in ophiolites may form by lightning strikes" by Griffin et al., 2018: No evidence for transition zone metamorphism in the Luobusa ophiolite. *Geochemical Perspectives Letters*, **7**, 3–4.

Ballhaus C., Helmy H.M., Fonseca R.O.C., Wirth R., Schreiber A.L. and Jöns N. (2021) Ultra-reduced minerals in ophiolites cannot come from Earth's mantle. *American Mineralogist*, **106**, 1053–1063.

Burla M.C., Caliandro R., Carrozzini B., Cascarano G.L., Cuocci C., Giacovazzo C., Mallamo M., Mazzone A. and Polidori G. (2015) Crystal structure determination and refinement via SIR2014. *Journal of Applied Crystallography*, **48**, 306–309.

Chesnokov B.V., Lotova E.V., Nigmatullina E.N., Pavlutchenko V.S. and Bushmakin A.F. (1990) Dmisteinbergite, $CaAl_2Si_2O_8$, (hexagonal), a new mineral. *Zapiski Vsesoyuznogo Mineralogicheskogo Obshchestva*, **119**, 43–46 [in Russian].

Cliff G. and Lorimer G.W. (1975). The quantitative analysis of thin specimens. *Journal of Microscopy*, **103**, 203–207.

Davis G.L. and Tuttle O.F. (1952) Two new crystalline phases of the anorthite composition, $CaO \cdot Al_2O_3 \cdot 2SiO_2$. *American Journal of Science, Bowen Volume*, **1952**, 107–114.

Dimitrijević R., Dondur V. and Kremenović A. (1996) Thermally induced phase transformations of Ca-exchanged LTA and FAU zeolite frameworks: Rietveld refinement of the hexagonal $CaAl_2Si_2O_8$ diphyllosilicate structure. *Zeolites*, **16**, 294–300.

Di Pierro S. and Gnos E. (2016) Ca-Al-silicate inclusions in natural moissanite (SiC). *American Mineralogist*, **101**, 71–81.

Fintor K., Park C., Nagy S., Pál-Molnár E. and Krot A.N. (2014) Hydrothermal origin of hexagonal $CaAl_2Si_2O_8$ (dmisteinbergite) in a compact type A CAI from the Northwest Africa 2086 CV3 chondrite. *Meteoritics & Planetary Science*, **49**, 812–823.

Gagné O.C. and Hawthorne F.C. (2016) Chemographic exploration of the milarite-type structure. *The Canadian Mineralogist*, **54**, 1229–1247.

Gemmi M., Mugnaioli E., Gorelik T.E., Kolb U., Palatinus L., Boullay P., Hovmöller S. and Abrahams J.P. (2019) 3D Electron Diffraction: The Nanocrystallography Revolution. *ACS Central Science*, **5**, 1315–1329.

Goldsmith J.R. (1953) A "simplexity principle" and its relation to "ease" of crystallization. *Journal of Geology*, **61**, 439–451.

Griffin W.L., Gain S.E.M., Bindi L., Toledo V., Cámara F., Saunders M. and O'Reilly S.Y. (2018) Carmeltazite, $ZrAl_2Ti_4O_{12}$, a new mineral trapped in corundum from volcanic rocks of Mt Carmel, Northern Israel. *Minerals*, **8**, 601, doi:10.3390/min8120601

Griffin W.L., Gain S.E.M., Saunders M., Huang J.H., Alard O., Toledo V. and O'Reilly S.Y. (2022) Immiscible metallic melts in the upper mantle beneath Mount Carmel, Israel: Silicides, phosphides and carbides. *American Mineralogist*, **107**, 532–549.

Hawthorne F.C., Uvarova Y.A. and Sokolova E. (2019) A structure hierarchy for silicate minerals: sheet silicates. *Mineralogical Magazine*, **83**, 3–55. https://doi.org/10.1180/mgm.2018.152.

Hwang S.L., Shen P., Chu H.T., Yui T.F., Liou J.G., Sobolev N.V., Zhang R.Y., Shatsky V.S. and Zayachkovsky A.A. (2004) Kokchetavite: a new potassium-feldspar polymorph from the Kokchetav ultrahigh-pressure terrane. *Contributions to Mineralogy and Petrology*, **148**, 380–389.

Kanzaki M., Xue X.Y., Amalberti J. and Zhang Q. (2012) Raman and NMR spectroscopic characterization of high-pressure K-cymrite ($KAlSi_3O_8·H_2O$) and its anhydrous form (kokchetavite). *Journal of Mineralogical and Petrological Sciences*, **107**, 114–119.

Kolb U., Gorelik T., Kübel C., Otten M.T. and Hubert C. (2007) Towards automated diffraction tomography: Part I—Data acquisition. *Ultramicroscopy*, **107**, 507–513, https://doi.org/10.1016/j.ultramic.2006.10.007.

Kolb U., Mugnaioli E. and Gorelik T.E. (2011) Automated electron diffraction tomography - A new tool for nano crystal structure analysis. *Crystal Research and Technology*, **46**, 542–554, https://doi.org/10.1002/crat.201100036.

Kraus W. and Nolze G. (1996) POWDER CELL - a program for the representation and manipulation of crystal structures and calculation of the resulting X-ray powder patterns. *Journal of Applied Crystallography*, **29**, 301–303.

Krivovichev S.V. (2012) Topological complexity of crystal structures: quantitative approach. *Acta Crystallographica*, **A68**, 393–398.

Krivovichev S.V. (2013) Structural complexity of minerals: information storage and processing in the mineral world. *Mineralogical Magazine*, **77**, 275–326.

Krivovichev S.V. (2020) Feldspar polymorphs: diversity, complexity, stability. *Zapiski Rossiiskogo Mineralogicheskogo Obshchestva*, **149**(4), 16–66.

Krivovichev S.V., Shcherbakova E.P. and Nishanbaev T.P. (2012) The crystal structure of svyatoslavite and evolution of complexity during crystallization of a $CaAl_2Si_2O_8$ melt: A structural automata description. *The Canadian Mineralogist*, **50**, 585–592.

Krivovichev S.V., Krivovichev V.G., Hazen R.M., Aksenov S.M., Avdontceva M.S., Banaru A.M., Gorelova L.A., Ismagilova R.M., Kornyakov I.V., Kuporev I.V., Morrison S.M., Panikorovskii T.L. and Starova G.L. (2022) Structural and chemical complexity of minerals: an update. *Mineralogical Magazine*, **86**, 183–204.

Litasov K.D., Kagi H. and Bekker T.B. (2019a) Enigmatic super-reduced phases in corundum from natural rocks: Possible contamination from artificial abrasive materials or metallurgical slags. *Lithos*, **340–341**, 181–190.

Litasov K.D., Bekker T.B. and Kagi H. (2019b) Discussion. Reply to the discussion of "Enigmatic super-reduced phases in corundum from natural rocks: Possible contamination from artificial abrasive materials or metallurgical slags" by Litasov et al. [Lithos, v. 340–341, p. 181–190 by W.L. Griffin, V. Toledo and S.Y. O'Reilly. Lithos 340–341 (2019) 181–190. *Lithos*, **348–349**, 105170, https://doi.org/10.1016/j.lithos.2019.105170.

Ma C., Krot A.N. and Bizzarro M. (2013) Discovery of dmisteinbergite (hexagonal $CaAl_2Si_2O_8$) in the Allende meteorite: A new member of refractory silicates formed in the solar nebula. *American Mineralogist*, **98**, 1368–1371.

Mills S.J., Hatert F., Nickel E.H. and Ferraris G. (2009) The standardisation of mineral group hierarchies: application to recent nomenclature proposals. *European Journal of Mineralogy*, **21**, 1073–1080.

Momma K. and Izumi F. (2011) VESTA 3 for three-dimensional visualization of crystal, volumetric and morphology data. *Journal of Applied Crystallography*, **44**, 1272–1276.

Mugnaioli E. and Gemmi M. (2018) Single-crystal analysis of nanodomains by electron diffraction tomography: Mineralogy at the order-disorder borderline. *Zeitschrift für Kristallographie – Crystalline Materials*, **233**, 163–178.

Mugnaioli E., Gorelik T. and Kolb U. (2009) "Ab initio" structure solution from electron diffraction data obtained by a combination of automated diffraction tomography and precession technique. *Ultramicroscopy*, **109**, 758–765, https://doi.org/10.1016/j.ultramic.2009.01.011.

Palatinus L., Petříček V. and Corrêa C.A. (2015a) Structure refinement using precession electron diffraction tomography and dynamical diffraction: theory and implementation. *Acta Crystallographica*, **A71**, 235–244.

Palatinus L., Corrêa C.A., Steciuk G., Jacob D., Roussel R., Boullay P., Klementová M., Gemmi M., Kopeček J., Domeneghetti M.C., Cámara F. and Petříček V. (2015b) Structure refinement using precession electron diffraction tomography and dynamical diffraction: tests on experimental data. *Acta Crystallographica*, **B71**, 740–751.

Palatinus L., Brázda P., Boullay P., Perez O, Klementová M., Petit S., Eigner V., Zaarour M. and Mintova S. (2017) Hydrogen positions in single nanocrystals revealed by electron diffraction. *Science*, **355**, 166–169.

Palatinus L., Brázda P., Jelinek M., Hrda J., Steciuk G. and Klementová M. (2019) Specifics of the data processing of precession electron diffraction tomography data and their implementation in the program PETS2.0. *Acta Crystallographica*, **B75**, 512–522.

Petříček V., Dusek M. and Palatinus L. (2014) Crystallographic computing system JANA2006: General features. *Zeitschrift für Kristallographie*, **229**, 345–352.

Ribbe P.H. (1983) The chemistry, structure, and nomenclature of feldspars. Pp. 1–20 in: *Feldspar Mineralogy* (Ribbe, P.H., editor). Reviews in Mineralogy, Volume 2. Mineralogical Society of America, Washington DC.

Romanenko A.V., Raschchenko S.V., Sokol A.G., Korsakov A.V., Seryotkin Y.V., Glazyrin K.V. and Musiyachenko K. (2021) Crystal structures of K-cymrite and kokchetavite from single-crystal X-ray diffraction. *American Mineralogist*, **106**, 404–409.

Simakin A.G., Eremyashev V.E. and Kucherinenko Y.V. (2010) New data on dmisteinbergite. *Zapiski Rossiiskogo Mineralogicheskogo Obshchetstva*, **139** (3), 102–108 [in Russian].

Smith J.V. and Bailey S.W. (1963) Second review of A1-O and Si-O tetrahedral distances. *Acta Crystallographica*, **16**, 801–811.

Thompson P., Parsons I., Graham C.M. and Jackson B. (1998) The breakdown of potassium feldspar at high water pressures. *Contributions to Mineralogy and Petrology*, **130**, 176–186.

van Genderen E., Clabbers M.T.B., Das P.P., Stewart A., Nederlof I., Barentsen K.C., Portillo Q., Pannu N.S., Nicolopoulos S., Gruene T. and Abrahams J.P. (2016) Ab initio structure determination of nanocrystals of organic pharmaceutical compounds by electron diffraction at room temperature using a Timepix quantum area direct electron detector. *Acta Crystallographica*, **A72**, 236–242, https://doi.org/10.1107/S2053273315022500.

Vincent R. and Midgley P.A. (1994) Double conical beam-rocking system for measurement of integrated electron diffraction intensities. *Ultramicroscopy*, **53**, 271–282.

Wannhoff I., Ferrero S., Borghini A., Darling R. and O´Brien P.J. (2022) First evidence of dmisteinbergite ($CaAl_2Si_2O_8$ polymorph) in high grade metamorphic rocks. *American Mineralogist*, https://doi.org/10.2138/am-2022-8505.

Xiong Q., Griffin W.L., Huang J.-X., Gain S.E.M., Toledo V., Pearson N.J. and O'Reilly S.Y. (2017) Super-reduced mineral assemblages in "ophiolitic" chromitites and peridotites: the view from Mount Carmel. *European Journal of Mineralogy*, **29**, 557–570.

Xiong F., Xu X., Mugnaioli E., Gemmi M., Wirth R., Grew E.S., Robinson P.T. and Yang J. (2020) Badengzhuite, TiP, and zhiqinite, $TiSi_2$, two new minerals from the Cr-11 chromitite orebody, Luobusa ophiolite, Tibet, China: Evidence for super-reduced mantle-derived fluids? *European Journal of Mineralogy*, **32**, 557–574.

Xiong F., Xu X., Mugnaioli E., Gemmi M., Wirth R., Grew E.S. and Robinson P.T. (2022a) Jingsuiite, TiB_2, a new mineral from the Cr-11 podiform chromitite orebody, Luobusa ophiolite, Tibet, China: Implications for recycling of boron. *American Mineralogist*, **107**, 43–53.

Xiong F., Xu X., Mugnaioli E., Gemmi M., Wirth R., Yang J. and Grew E.S. (2022b) Wodegongjieite, IMA 2020-036b. CNMNC Newsletter 67. *Mineralogical Magazine*, **86**, https://doi.org/10.1180/mgm.2022.56

Xiong F., Xu X., Mugnaioli E., Gemmi M., Wirth R., Yang J. and Grew, E.S. (2022c) Wenjiite, $Ti_{10}(Si,P,o)_7$, and kangjinlaite, $Ti_{11}(Si,P)_{10}$, new minerals

in the ternary Ti–P–Si system from the Luobusa ophiolite, Tibet, China. *American Mineralogist*, https://doi.org/10.2138/am-2022-8226.

Xu X., Yang J., Chen S., Fang Q. and Bai W. (2009) Unusual mantle mineral group from Chromitite Orebody Cr-11 in Luobusa Ophiolite of Yarlung-Zangbo Suture Zone, Tibet. *Journal of Earth Science*, **20**, 284–302.

Xu X.Z., Yang J.S., Robinson P.T., Xiong F.H., Ba D.Z. and Guo G.L. (2015). Origin of ultrahigh pressure and highly reduced minerals in podiform chromitites and associated mantle peridotites of the Luobusa ophiolite, Tibet. *Gondwana Research*, **27**, 686–700.

Zolotarev A.A., Krivovichev S.V., Panikorovskii T.L., Gurzhiy V.V., Bocharov V.N. and Rassomakhin M.A. (2019) Dmisteinbergite, $CaAl_2Si_2O_8$, a metastable polymorph of anorthite: Crystal-structure and Raman spectroscopic study of the holotype specimen. *Minerals*, **9**, 570, https://doi.org/10.3390/min9100570.